



ELSEVIER

Physica B 221 (1996) 238–244

PHYSICA B

The structure and phase behavior of electrodeposited halides on single-crystal metal surfaces

B.M. Ocko^{a,*}, O.M. Magnussen^a, J.X. Wang^b, R.R. Adžić^b, Th. Wandlowski^c^a Department of Physics, Brookhaven National Laboratory, Upton, NY 11790, USA^b Department of Applied Science, Chemical Sciences Division, Brookhaven National Laboratory, Upton, NY 11790, USA^c Department of Electrochemistry, University of Ulm, D-89069 Ulm, Germany

Abstract

Synchrotron X-ray scattering results of halide monolayers of bromide and iodide on single-crystal electrodes are presented. Both commensurate and incommensurate structures are observed. The incommensurate structures electrocompress with increasing potential. The relative roles of the halide–halide and the substrate–halide interactions are discussed for iodide on Au(111), Ag(111), and Pt(111) and for bromide on Au(111), Ag(111) and Au(100).

1. Introduction

A true atomistic picture of the electrode interface is starting to emerge. This development is primarily due to the introduction of in situ structural methods, specifically, scanning tunneling microscopy (STM), atomic force microscopy (AFM), and X-ray techniques, including surface X-ray scattering (SXS). Studies using these techniques have shown that electrode surfaces are well ordered with coherence lengths of several hundred Angstroms and that the sharp features observed using classical electrochemical techniques are correlated with adlayer phase transitions. Here we review recent SXS results of halide adlayers on low index faces of gold, silver, and platinum, with particular emphasis on the nature of the potential dependence of incommensurate phases, and on the effect of the substrate metal and crystallographic orientation on the adlayer structure.

Investigations of electrode surfaces using X-ray scattering techniques have benefitted from the development of thin-layer electrochemical cells and high-intensity, synchrotron X-ray sources. The first successful X-ray scattering measurements from a well-defined surface showed that incommensurate hexagonal monolayers of lead form at potentials positive of the bulk Nernst potential and that

these monolayers electrocompress with decreasing potential [1]. Whereas these pioneering studies were carried out on epitaxial gold and silver films on Mica, most recent studies have utilized single-crystal surfaces. These experiments have investigated the electrodeposited monolayers of Bi on Ag(111) [2] and Au(111) [3], Tl on Ag(111) [4], Au(111) [5], Au(100) [6], and Ag(100) [7], and Pt(111) [8], and Pb on Ag(111) [1], Pt(111) [9] and Au(100) [10] as well as adsorbed halide monolayers on Au(111) [11, 12], Au(100), Au(110) and Pt(111) [13]. They revealed well-ordered adlayer structures, often incommensurate with the substrate with potential-dependent lattice parameters. Scattering measurements have also shown that at sufficiently negative potentials the (111), (100), and (110) surfaces of gold reconstruct in a similar manner as the same surfaces in vacuum and that a transformation to a (1 × 1) state occurs at higher potentials [14–18]. In addition, studies have also been carried out of the ionic adsorption of alkali-halide adlayers [19], the roughening of platinum [20], the relaxation of the Pt(111) surface [21], the interfacial water structure on Au(111) [15, 22] and Ag(111) [23]. Several reviews pertaining to in situ X-ray studies under electrochemical conditions are recommended [22, 24–28].

The structure of adsorbed monolayers and, in particular, the registry between the adlayer and the substrate is affected by the symmetry of the substrate, the adsorbate–adsorbate

* Corresponding author.

interactions, and the corrugations in the adsorbate–substrate interaction potential [29–34]. The latter increases for more open surfaces, i.e., for FCC surfaces in the order (111), (100), (110). A simple one-dimensional model of harmonically bound atoms in a sinusoidal corrugation potential given by Frankel and Kontorowa [29] and by Frank and Van der Merwe [30] showed that the lowest-energy solution can give rise to domain walls (solitons). The spacing and widths of these domain walls are determined by the lattice mismatch and the ratio of corrugation and lateral interaction energy. In the limit of sharp domain walls, most of the adatoms occupy highly coordinated, commensurate positions except at domain walls where they are in energetically less-favorable sites. Here we will refer to this structure as a domain-wall incommensurate phase. On the other hand, when the domain walls are diffuse, such that the atoms are equally spaced along the incommensurate direction we will refer to this structure as a uniformly compressed incommensurate phase. Often, both of these structures are referred to as striped phases where the height modulation provides a stripe-like appearance. For the case of the domain-wall phase the stripes are narrow and for the uniformly compressed phase the stripes are broad. Finally, we note that incommensurate phases are more likely to appear on the close-packed (111) surface.

An extensively studied model system for the phase behavior of two-dimensional adsorbates is the physisorption of noble gases on the cleaved, hexagonal face of graphite [35]. Here the chemical potential can be varied through the vapour pressure and clean, well-defined surfaces can be prepared in a simple way. In contrast to cleaved surfaces such as graphite, metal and semiconductor surfaces can be prepared with arbitrary crystallographic orientations. Thus, they are ideally suited for investigating the role of the crystallographic orientation on the phase behavior of adsorbates. However, most adsorbates are chemisorbed making the experimental control of the adsorbates chemical potential through its vapour pressure extremely difficult [31]. Rather, the coverage in gas-phase experiments is varied by dosing the sample to a well defined coverage.

Under electrochemical conditions a wide variety of cation and anion species, with varying interactions and sizes, can be electrodeposited as monolayers and as bulk. Here, the chemical potential of the adsorbate can be directly and accurately controlled through the applied potential. In addition, the substrate metal and crystallographic orientation can be varied. As a result, the electrochemical environment can provide an important testing ground for fundamental issues in two-dimensional physics and in particular the nature of the commensurate–incommensurate transition. From a surface physics perspective, one disadvantage of the electrochemical environment is that the temperature cannot be varied over a wide range.

2. Examples

The results of X-ray scattering studies of the adsorption of iodide and bromide on gold and silver single-crystal surfaces are summarized below. Potentials are referenced to a Ag/AgCl(3M NaCl) reference electrode. The adsorption of halides can be monitored using cyclic voltammetry (CV) which measures the rate of charge transfer at a fixed potential sweep rate. The initial adsorption gives rise to a broad peak in the CV which is often followed by several sharp peaks at higher potentials [12, 36–38]. The first sharp peak in the CV is usually interpreted as a transition from a disordered adlayer to an ordered adlayer. The additional peaks correspond to transitions between different ordered structures. All of the ordered halide adlayers form over a potential regime where the underlying surfaces are unreconstructed. For all halides studied to date, the coverages deduced from the X-ray measurements shift by 59 ± 5 mV per decade change in the halide solution concentration [12, 11]. From this we conclude that the adsorbed halides are almost completely discharged in the ordered phases. In addition, the adsorbed halides are atomic and they do not exhibit diatomic characteristics. Finally, we point out that no effect of the cation species (Li^+ , Na^+ , K^+ , and Cs^+) on the phase behavior was observed in the measurements presented here.

2.1. Iodide on Au(111) and Ag(111)

In the first example we consider the adsorption of iodide on the (111) faces of Au and Ag. Iodine is the largest, most polarizable, and most strongly adsorbing of the halides and exhibits ordered phases over the widest potential region. Since silver and gold have nearly identical lattice constants, a comparison of the iodide-phase behavior allows us to focus on the relative role of the substrate–halide interaction.

With increasing potential, the adsorption of iodide on Ag(111) gives rise to the series of ordered structures shown in Fig. 1(a) [39]. These correspond to the commensurate $(\sqrt{3} \times \sqrt{3})R30^\circ$, the uniaxial-incommensurate $c(p \times \sqrt{3})$, and the rotated-hexagonal phases where the coverage, θ , extends from $\frac{1}{3}$ in the commensurate phase to 0.442 at the most positive potentials. In the $c(p \times \sqrt{3})$ structure the iodide atoms are arranged in a centered rectangular unit cell with sides $\sqrt{3}$ and p , where p decreases with increasing potential. By construction the coverage θ , corresponding to this unit cell, is equal to p^{-1} . In addition, all of the iodide atoms reside in the rows of the gold. The absence of satellite peaks – expected for sharp domain walls [40] – leads us to the conclusion that the phase is better described as uniformly compressed rather than a domain-wall phase. In the rotated-hexagonal phase $\theta = |a_{\text{Ag}}/a_1|^2$, where a_1 is the potential-dependent I–I separation and $a_{\text{Ag}} = 2.889 \text{ \AA}$ is the Ag–Ag spacing.

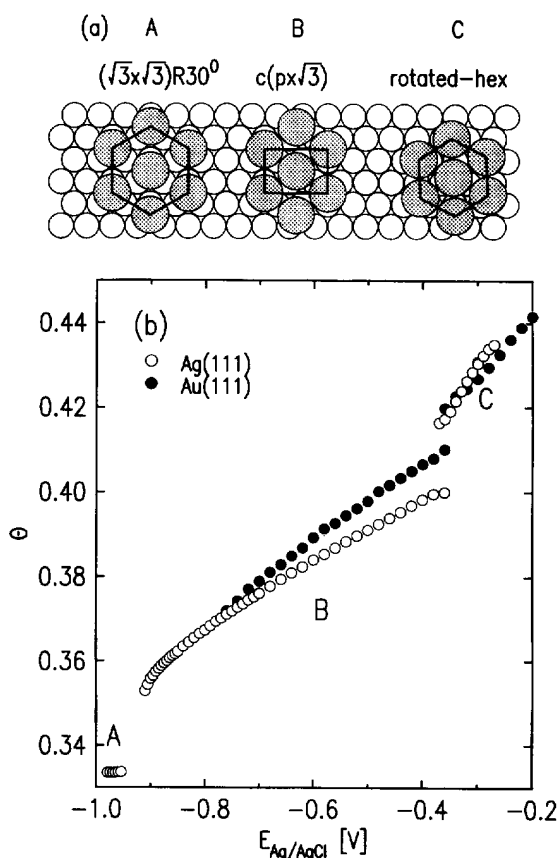


Fig. 1. (a) The structures of iodide on Ag(111) and Au(111) deduced from surface X-ray scattering results. They correspond to A: the commensurate $(\sqrt{3} \times \sqrt{3})R30^\circ$, B: the uniaxial-incommensurate $c(p \times \sqrt{3})$, and C: the rotated-hexagonal phases. (b) The potential-dependent coverages, θ , of iodide, determined from the in-plane diffraction, are shown versus the applied potential for Ag(111) in 0.1 M NaI and for Au(111) in 0.1 M KI. The potential scale of the Au(111) data has been shifted negatively by 0.5 V to facilitate the comparison with the Ag(111) data.

In Fig. 1(b) the potential-dependent iodide coverage on the Ag(111) surface in 0.1 M NaI is shown as open circles [41]. The commensurate phase is stable from about -0.9 to -0.94 V. No ordered iodide phase is observed below -1.0 V. The $c(p \times \sqrt{3})$ incommensurate phase exists between -0.92 and -0.36 V. Here θ continuously increases from about 0.355 and to 0.40. We note that it is difficult to determine the coverage between $\frac{1}{3}$ and 0.355 due to the overlap of the diffraction peaks from the three symmetry equivalent domains which cannot be easily resolved. At the most positive extreme of the $c(p \times \sqrt{3})$ phase, the structure corresponds to the $(5 \times \sqrt{3})$ high-order commensurate unit cell with a nearest-neighbor iodide spacing of 4.39 \AA .

Upon a slight further increase in potential, the $(5 \times \sqrt{3})$ phase vanishes and a rotated-hexagonal phase forms with

$\theta = 0.417$ corresponding to $a_l = 4.59 \text{ \AA}$. The positive potential range of this phase is limited by the onset of bulk AgI formation.

We now contrast the iodide on Ag(111) phase behavior with that on Au(111) [12] in 0.1 M KI, shown in Fig. 1(b) as filled circles, where the gold lattice constant, $a_{Au} = 2.885 \text{ \AA}$ is slightly smaller than a_{Ag} . For comparison purposes, the potential scale of the results on Au(111) have been shifted by -0.50 V. This shift is a manifestation of the much more negative potential of zero charge of silver compared to gold. The commensurate phase is never observed on Au(111), rather it is intercepted by the disordered (fluid) phase at the potentials where it would be expected. As demonstrated in Fig. 1, similar phase behavior on the two metals is observed in the $c(p \times \sqrt{3})$ and the rotated-hexagonal phases. In the $c(p \times \sqrt{3})$ phase the maximum coverage and the electrocompressibility, $d\theta/dE$ are slightly smaller on silver than gold. Here the electrocompressibility has the opposite sign as for metal deposition since the halide and metal ions have the opposite charge. As with I on Ag(111), the absence of satellite peaks implies that the structure is a uniformly compressed rather than a domain-wall phase. Almost identical behavior is observed in the rotated-hexagonal phase which suggests that the influence of the substrate is minimal within this phase. The coverages in the rotated-hexagonal phase are nearly identical to those on Ag(111).

Many aspects of the observed phase behavior can be understood in terms of the adjustable electrochemical potential which favors increased surface densities at higher potentials, and the competition between the adsorbate–adsorbate interaction and the adsorbate–substrate interaction. In the uniaxial-incommensurate phase the adsorbates reside between the rows of the substrate atoms and this configuration has a lower interfacial energy than the rotated-hexagonal phase where some of the adsorbates must be in high-energy atop sites. However, the uniaxial-incommensurate phase is slightly distorted from the hexagonal configuration and this distortion increases the adsorbate–adsorbate elastic interaction energy. With increasing potential the distortion increases and at a critical potential the uniaxial-incommensurate phase transforms into the incommensurate, rotated-hexagonal phase.

The phase behavior of iodide on Ag(111) is especially significant since it elegantly displays the loss of commensuration with two distinct phase transformations with increasing potential. This phase sequence has been predicted by Bak and coworkers [42] using Landau theory. Similar results have also been obtained by Kardar [43] using a generalized three-state Potts model.

Finally, we contrast the results of iodide on Ag(111) and Au(111) with those on Pt(111). These studies have been carried out using ex situ LEED [44], in situ STM [45] and with SXS in our laboratory. All of these studies have shown the existence of a (3×3) phase with $\theta = \frac{4}{9}$ and a

$(7 \times 7)R 21.8^\circ$ structure with $\theta = 3/7 = 0.428$. The exact phase behavior between these two phases could not be reproducibly determined in these studies. Since $a_{\text{Pt}} = 2.77 \text{ \AA}$, the iodide densities are much higher on Pt than either Ag or Au. In fact, the nearest-neighbor iodide separations equal 4.16 and 4.25 \AA in the (3×3) and $(7 \times 7)R 21.8^\circ$ phases, respectively. This is about 0.1–0.2 \AA smaller than observed on Ag or Au. This indicates that the Pt–I interaction is stronger than for Au–I or Ag–I.

2.2. Bromide on Au(111) and Au(100)

Bromide is slightly smaller and less strongly adsorbed on metal surfaces than iodide. Here we compare the results of Br on the (111) and (100) surfaces of gold. On the Au(111) electrode, electrodeposited Br forms a rotated-hexagonal phase [11] (see the top of Fig. 2) which is the same phase as the high potential phase of iodide on Au(111). In Fig. 2 we show the potential-dependent Br coverage in 0.1 M NaBr. The rotated-hexagonal diffraction pattern appears when the potential is raised into the range positive of 0.42 V. Between 0.42 and 0.72 V the Br coverage normalized to that of the substrate, θ , increases from 0.465 to 0.515 whereas the absolute coverage increases from 6.46×10^{14} to $7.16 \times 10^{14} \text{ cm}^{-2}$. The atomic Br–Br spacing, a_{Br} , decreases from 4.24 \AA at 0.42 V to the saturation value of 4.03 \AA at the highest potentials. The electrocompression of the adlayer proceeds monotonically and there are no discontinuities in the adatom–adatom spacings. Hence, we can exclude a lock-in of the adlayer into high-order commensurate structures, which would result in a fixed bromide spacing over a range of potentials. Whereas the uniaxial-incommensurate phase is observed at potentials negative of the rotated-hexagonal phase for I on Au(111), no such phase is observed for Br. Thus, the rotated-hexagonal phase directly transforms to the liquid phase below 0.42 V.

In the rotated-hexagonal phase, electrochemical measurements of the coverage using chronocoulometric techniques [47] are in reasonable agreement with the data shown in Fig. 2 and this agreement increases our confidence in both techniques. The electrochemical measurements were also carried out in the disordered phase and they show that the electrocompressibility is similar on both sides of the transition.

On Ag(111), SXS studies have shown that Br forms a high-order commensurate $(7 \times 7)R 21.8^\circ$ structure with 25 Br atoms in the unit cell over an $\approx 100 \text{ mV}$ wide potential regime negative of the potential of bulk AgBr formation [48]. This structure has a spacing $a_{\text{Br}} = 4.04 \text{ \AA}$ and an absolute coverage, $\Gamma = 7.05 \times 10^{14} \text{ cm}^{-2}$, close to the maximum coverage found on Au(111). The commensurate nature and the different alignment as compared to Br on Au(111) indicates a stronger corrugation potential than on Au(111), in agreement with the trend established for

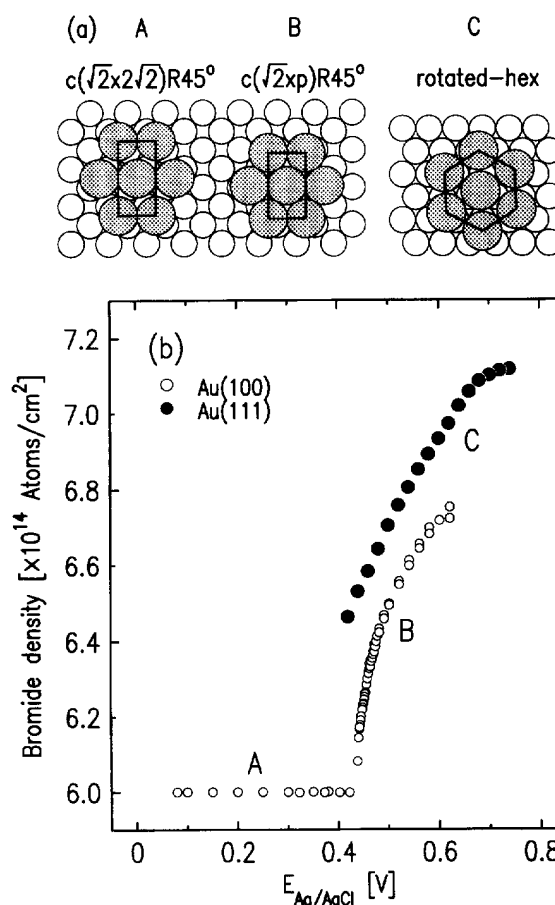


Fig. 2. (a) The structures of Br on Au(100) and Au(111). They correspond to A: the commensurate $c(\sqrt{2} \times 2\sqrt{2})R45^\circ$ structure, B: the uniaxial-incommensurate $c(\sqrt{2} \times p)R45^\circ$ structure, and C: the rotated-hexagonal structure. (b) The potential-dependent bromide coverages, Γ , in units of atoms/cm², on Au(100) and Au(111), determined from the in-plane diffraction, are shown versus the applied potential. The Au(100) and Au(111) studies were carried out in 0.05 M NaBr and 0.10 M NaBr solutions, respectively. This concentration difference causes a +0.018 V shift for the Au(111) data set.

iodide. For Br on Pt(111), an electrocompressive, aligned-hexagonal phase with a slightly higher maximum density, $\Gamma = 7.6 \times 10^{14} \text{ cm}^{-2}$, has recently been reported [13].

How does the substrate structure affect the structure and coverage of the adsorbate? In order to explore this issue, we have carried out studies of the electrodeposition of Br on the Au(100) surface [46]. As shown in Fig. 2(a), this surface has an underlying square symmetry with a lattice spacing of 2.885 \AA which gives 1.20×10^{15} gold atoms/cm². This is 86.6% of the Au(111) density. In bromide containing solutions, we find at lower potentials a commensurate $c(\sqrt{2} \times 2\sqrt{2})R45^\circ$ phase (see Fig. 2(b)) with $\theta = \frac{1}{2}$. This

commensurate structure contains two atoms in a rectangular unit cell with sides 4.08 Å and 8.16 Å. By construction, the nearest-neighbor separations are 4.08 and 4.56 Å. This phase is unusual since the atoms reside on bridge sites rather than the more coordinated fourfold hollows sites. The latter coordination is found for the $(\sqrt{2} \times \sqrt{2})R45^\circ$ phase, often referred to as $c(2 \times 2)$, which also has $\theta = \frac{1}{2}$ and is more commonly observed on FCC (100) surfaces. However, the symmetry of this phase is square, whereas the $c(\sqrt{2} \times 2\sqrt{2})R45^\circ$ phase is closer to hexagonal. The preference for the $c(\sqrt{2} \times 2\sqrt{2})R45^\circ$ phase suggests that the elastic interactions between the relatively large Br adsorbates, which favor hexagonal packing, are more significant than the adsorbate–substrate interaction energy difference between the two phases.

Above 0.42 V in 0.05 M NaBr, the $c(\sqrt{2} \times 2\sqrt{2})R45^\circ$ transforms to a uniaxial-incommensurate $c(\sqrt{2} \times p)R45^\circ$, where $p = 2\sqrt{2}/(1 + \varepsilon)$ and ε is a measure of the incommensurability and varies continuously between 0 and 0.12 over the potential range 0.42–0.60 V, respectively. In Fig. 2(b) the potential-dependent coverage, Γ , shown as circles, is proportional to $1 + \varepsilon$. Whereas the nearest-neighbor distance is always 4.08 Å, the next-nearest-neighbor spacing decreases from 4.56 Å for $\varepsilon = 0$ (commensurate) to 4.13 Å when $\varepsilon = 0.12$. Thus, the distortion from hexagonal symmetry, determined from the ratio between the nearest-neighbor and next-nearest-neighbor distances, decreases from 11.7% to 1.2% over the measured range. Despite the small distortion at this potential, the coverage at 0.60 V on the Au(111) face is still 3% higher than on the (100) face. The positive potential ranges are limited by the stability of the gold with respect to Br-induced dissolution. Consequently, the more densely packed (111) face is more stable than the more open (100) face and the (111) data extends to higher potentials.

No satellite peaks have been observed for Br on Au(100) within the limits of the diffuse scattering background. This allows us to establish that the satellite peaks are at least a factor of 50 lower than the principal Br peaks when ε is greater than 0.05. With this limitation, we have analyzed the scattering data in terms of locally commensurate regions separated by domain walls and deduced that the domain wall width must be nearly as wide as the separation between domain walls. Thus, the incommensurate phase is better defined by a uniformly compressed phase rather than a domain-wall phase.

In contrast to the order/disorder transition observed at lower potentials and the uniaxial-incommensurate to rotated-hexagonal transition for iodide on Au(111) and Ag(111), the coverage in the neighborhood of the commensurate–incommensurate transition varies continuously. Accordingly, this transition is a second-order phase transition. The measured critical exponent, β , which describes the behavior of incommensurability versus the potential, has been

obtained by fitting the incommensurability to the form $\varepsilon = (E - E_0)^\beta$ in the incommensurate phase. When the entire range is used in the fitting $\beta = 0.4 \pm 0.02$; however systematic deviations from this form are evident. When the range is restricted to $\varepsilon < 0.04$, the data is consistent with $\beta = \frac{1}{2}$. The dependence of β on the range is a direct consequence of the saturation which occurs when the bromide–bromide separation approaches the Van der Waals diameter.

In the standard model of the commensurate–incommensurate transition the commensurate phase transforms into a striped incommensurate phase. As described by Pokrofsky and Talapov [49], the appearance of entropically wandering, non-interacting domain walls marks the transition and they predict that $\beta = \frac{1}{2}$. Measurements of the commensurate–incommensurate transition for noble gases on graphite [35] Xe on Pt(111) [33], and bromine intercalated graphite [50] have confirmed the predicted exponent. Since the model of Pokrofsky and Talapov assumes sharp domain walls rather than uniform compression, this model does not appear directly applicable to Br on Au(100) over most of the measured potential range. It may, however, apply close to the transition where ε is small and the diffraction intensities are weak. Consequently, within this region it is difficult to distinguish between uniform compression and sharp domain walls.

As indicated by Fig. 2(b), ordered phases are more favorable on Au(100) than on Au(111) since the $c(\sqrt{2} \times 2\sqrt{2})R45^\circ$ structure on Au(100) appears at 0.05 V, whereas the rotated-hexagonal structure on Au(111) only appears at 0.42 V. The small difference in bromide concentration in these studies accounts for a 0.018 V shift, albeit in the wrong direction. Thus, it is not responsible for the 0.37 V shift. Furthermore, differences between the respective potentials of zero charge (discussed below) cannot explain this shift. Rather, the difference is clearly a manifestation of the stronger bonding of Br to the more open (100) surface.

Over a range of coverages, between about 6.45×10^{14} to 6.70×10^{14} cm⁻², the close-packed Br monolayers on Au(100) and Au(111) exhibit similar electrocompressibilities, albeit a potential shift of 0.1 V. The similarity in the potential dependences, despite the uniaxial-compression on Au(100) compared to the biaxial compression on Au(111), suggests that the interactions between the Au and Br are similar in both cases and that the symmetry of the substrate does not play a critical role at the highest coverages.

3. Summary

Our X-ray scattering studies of halides on the surfaces of gold and silver clearly show the existence of well-ordered monolayers over a wide potential regime. These studies have revealed that the halides tend to form

incommensurate phases which electrocompress. The in-plane separations are close to the van der Waals diameter. The absence of satellite peaks indicates that the incommensurate phases are uniformly compressed and do not correspond to domain-wall phase. Many aspects of the observed phase behavior can be understood in terms of a competition between the elastic adatom–adatom interactions and the adsorbate–substrate interaction.

The phase behavior of iodide on Au(1 1 1) and Ag(1 1 1) are rather similar. Both exhibit uniaxial-incommensurate and rotated-hexagonal phases which electrocompress. The existence of the commensurate ($\sqrt{3} \times \sqrt{3}$)R30° and ($5 \times \sqrt{3}$) phases on Ag(1 1 1) and not on Au(1 1 1) indicates that a stronger corrugation potential for halides on silver than on gold. For bromide, only an incommensurate phase is observed on Au(1 1 1). An ordered bromide phase forms on Au(1 0 0) at much more negative potentials indicating a somewhat stronger adsorbate-substrate interaction than on Au(1 1 1). The transition to the incommensurate $c(\sqrt{2} \times p)$ R45° phase and the potential-dependent incommensurability cannot be fully explained by existing theories of the commensurate–incommensurate transition.

Note added in proof: Complementary results for I on Ag(1 1 1) have recently been obtained by Yamada and coworkers using in situ STM and ex situ LEED [51].

Acknowledgements

This work is supported by the Division of Materials and Chemical Sciences, U.S. Department of Energy, under Contract No. DE-AC02-76CH00016. Financial support by the Deutsche Forschungsgemeinschaft (T.W.) and by the Weizmann Institute of Science through a Rosie and Max Varon Professorship (B.O) is gratefully acknowledged.

References

- [1] M.G. Samant, M.F. Toney, G.L. Borges, L. Blum and O.R. Melroy, *J. Phys. Chem.* 92 (1988) 220; O.R. Melroy, M.F. Toney, G.L. Borges, M.G. Samant, J.B. Kortright, P.N. Ross and L. Blum, *Phys. Rev. B* 38 (1988) 10962.
- [2] M.F. Toney, J.G. Gordon, M.G. Samant, G.L. Borges, D.G. Wiesler, D. Yee and L.B. Sorensen, *Langmuir* 7 (1991) 796.
- [3] C.H. Chen, K.D. Kepler, A.A. Gewirth, B.M. Ocko and J. Wang, *J. Phys. Chem.* 97 (1993) 7290.
- [4] M.F. Toney, J.G. Gordon, L. Kau, G.L. Borges, O.R. Melroy, M.H. Samant, D. Wiesler, D. Yee and L.B. Sorensen, *Phys. Rev. B* 42 (1990) 5594; M.F. Toney, J.G. Gordon, M.H. Samant, G.L. Borges, O.R. Melroy, M.H. Samant, D. Yee and L.B. Sorensen, *Phys. Rev. B* 45 (1992) 9362.
- [5] J.X. Wang, R.R. Adžić and B.M. Ocko, *J. Phys. Chem.* 98 (1994) 3182.
- [6] J.X. Wang, R.R. Adžić, O.M. Magnussen and B.M. Ocko, *Surf. Sci.* 335 (1995) 120.
- [7] J.X. Wang, R.R. Adžić, O.M. Magnussen and B.M. Ocko, *Surf. Sci.* 344 (1995) 111.
- [8] R.R. Adžić, J.X. Wang, O.M. Magnussen and B.M. Ocko, unpublished.
- [9] R.R. Adžić, J. Wang, C.M. Vitus and B.M. Ocko, *Surf. Sci. Lett.* 293 (1993) 876.
- [10] K.M. Robinson and W.E. O' Grady, *Faraday Discussions* 95 (1993) 55.
- [11] O.M. Magnussen, B.M. Ocko, J.X. Wang and R.R. Adžić, *Phys. Rev. B* 51 (1995) 5510; O.M. Magnussen et al., to be published in *J. Phys. Chem.*
- [12] B.M. Ocko, G.M. Watson and J. Wang, *J. Phys. Chem.* 98 (1994) 897; J. Wang, G.M. Watson and B.M. Ocko, *Physica A* 200 (1993) 751.
- [13] C.A. Lucas, N.M. Marković and P.N. Ross, *Surf. Sci. Lett.* 340 (1995) 949.
- [14] B.M. Ocko, J. Wang, A. Davenport and H. Isaacs, *Phys. Rev. Lett.* 65 (1990) 1466.
- [15] J. Wang, B.M. Ocko, A.J. Davenport and H.S. Isaacs, *Phys. Rev. B* 46 (1992) 10321.
- [16] B.M. Ocko, G. Helgesen, B. Schardt, J. Wang and A. Hamelin, *Phys. Rev. Lett.* 69 (1992) 3350.
- [17] I.M. Tidswell, N.M. Markovic, C.A. Lucas and P.N. Ross, *Phys. Rev. B* 47 (1993) 16542.
- [18] K.M. Robinson and W.E. O' Grady, *Rev. Sci. Instr.* 64 (1993) 1061.
- [19] J.X. Wang, G.M. Watson and B.M. Ocko, unpublished.
- [20] H. You and Z. Nagy, *Physica B* 198 (1994) 187.
- [21] I.M. Tidswell, N.M. Markovic and P.N. Ross, *Phys. Rev. Lett.* 71 (1993) 1601.
- [22] B.M. Ocko and J. Wang, *Synchrotron Techniques in Interfacial Electrochemistry*, eds. C.A. Melendres and A. Tadjeddine (Kluwer, Dordrecht, 1994) p. 127.
- [23] M.F. Toney, J.N. Howard, J. Richer, G.L. Borges, J.G. Gordon, O.R. Melroy, D. Wiesler, D. Yee and L.B. Sorensen, *Nature* 368 (1994) 444.
- [24] M.F. Toney, J.G. Gordon and O.R. Melroy, *SPIE Proc.* 1550 (1991) 140.
- [25] M.F. Toney and O.R. Melroy, in: *Electrochemical Interfaces: Modern Techniques for In-Situ Interface Characterization*, ed. H.D. Abruna (VCH Verlag, Berlin, 1991) p. 57.
- [26] M.F. Toney, *Synchrotron Techniques in Interfacial Electrochemistry*, eds. C.A. Melendres and A. Tadjeddine (Kluwer, Dordrecht, 1994) p. 109.
- [27] B.M. Ocko, O.M. Magnussen, J.X. Wang and R.R. Adžić, in: *Nanoscale Probes of the Solid/Liquid Interface*, eds. A.A. Gewirth and H. Siegenthaler (Kluwer, Dordrecht, 1995) p. 103.
- [28] M.F. Toney, J.G. Gordon, M.G. Samant, O.R. Melroy, D. Yee and L.B. Sorensen, *J. Phys. Chem.* 99 (1995) 4733.
- [29] Y.I. Frenkel and T. Kontorowa, *Zh. Eksp. Teor. Fiz.* 8 (1938) 1340.
- [30] F.C. Frank and J.H. Van der Merwe, *Proc. Roy. Soc. London* 198 (1949) 205.
- [31] A. Zangwill, *Physics at Surfaces* (Cambridge Univ. Press, Cambridge, 1988).
- [32] P.M. Chaiken and T.C. Lubensky, *Principles of Condensed Matter Physics* (Cambridge Univ. Press, Cambridge, 1995).

- [33] K. Kern and G. Cosma, in: *Chemistry and Physics of Solids VII*, eds. R. Vanselow and R.F. Howe (Springer, Berlin, 1988) p. 65.
- [34] B.N.J. Persson, *Surf. Sci. Rep.* 15 (1992) 1.
- [35] See, for instance, K.L. D'Amico, J. Bohr, D.E. Moncton and D. Gibbs, *Phys. Rev. B* 41 (1990) 4368.
- [36] A. Hamelin and J.P. Bellier, *J. Electroanal. Chem.* 41 (1973) 179.
- [37] D.A. Scherson and D.M. Kolb, *J. Electroanal. Chem.* 176 (1984) 353.
- [38] X. Gao and M.J. Weaver, *J. Am. Chem.* 114.
- [39] O.M. Magnussen, J.X. Wang and B.M. Ocko, unpublished.
- [40] P. Fenter and T.M. Lu, *Surf. Sci.* 154 (1985) 15.
- [41] O.M. Magnussen, B.M. Ocko and J.X. Wang, *J. Phys. Chem.*, unpublished.
- [42] P. Bak, D. Mukamel, J. Villain and K. Wentowska, *Phys. Rev. B* 19 (1979) 1610.
- [43] M. Kardar and A.N. Berker, *Phys. Rev. Lett.* 48 (1982) 1552.
- [44] J.L. Stickney, S.D. Rosasco, D. Song, B.C. Schardt and A.T. Hubbard, *Surf. Sci.* 130 (1983) 326.
- [45] B.C. Schardt, S.L. Yau and F. Rinaldi, *Science* 243 (1989) 1050.
- [46] Th. Wandlowski, J.X. Wang, O.M. Magnussen and B.M. Ocko, *J. Phys. Chem.*, submitted; B.M. Ocko et al., *Phys. Rev. B* 53 (1996).
- [47] J. Lipkowski, private communication.
- [48] O.M. Magnussen, J.X. Wang and B.M. Ocko, unpublished.
- [49] V.L. Pokrofsky and A.L. Talapov, *Phys. Rev. Lett.* 42 (1979) 66.
- [50] S.G.J. Mochrie, A.R. Kortan, R.J. Birgeneau and P.M. Horn, *Z. Phys.* 62 (1985) 79.
- [51] T. Yamada et al., to be published in *Surf. Sci.*